

# Finding eV-scale Light Relics with Cosmological Observables

Nicholas DePorzio,<sup>1</sup> Weishuang Linda Xu,<sup>1</sup> Julian B. Muñoz,<sup>1</sup> and Cora Dvorkin<sup>1</sup>

<sup>1</sup>*Department of Physics, Harvard University, Cambridge, MA 02138, USA*

Cosmological data provide a powerful tool in the search for physics beyond the Standard Model (SM). An interesting target are light relics, new degrees of freedom which decoupled from the SM while relativistic. Nearly massless relics contribute to the radiation energy budget, and are commonly searched through variations in the effective number  $N_{\text{eff}}$  of neutrino species. Additionally, relics with masses on the eV scale (meV-10 eV) become non-relativistic before today, and thus behave as matter instead of radiation. This leaves an imprint in the clustering of the large-scale structure of the universe, as light relics have important streaming motions, mirroring the case of massive neutrinos. Here we forecast how well current and upcoming cosmological surveys can probe light massive relics (LiMRs). We consider minimal extensions to the SM by both fermionic and bosonic relic degrees of freedom. By combining current and upcoming cosmic-microwave-background and large-scale-structure surveys, we forecast the significance at which each LiMR, with different masses and temperatures, can be detected. We find that a very large coverage of parameter space will be attainable by upcoming experiments, opening the possibility of exploring uncharted territory for new physics beyond the SM.

## I. INTRODUCTION

The nature of the dark sector is one of the major puzzles of fundamental physics, integral to the understanding of our universe across almost every epoch. Searches for the composition of the dark sector and, more broadly, of physics beyond the Standard Model (SM), take place at different energy scales, and use data ranging from particle colliders to astrophysical and cosmological surveys. The interactions of the dark sector with the SM are central to many of these searches. Yet, the small energies and interaction cross-sections expected in many models often result in low experimental sensitivity to new physics. In contrast, by exploring the entropic effects of new dark-sector physics, cosmological data is in an exciting position to make robust discoveries.

Numerous extensions of the SM happen to posit the existence of light, feebly interacting particles, including axions and axion-like particles [1–4], dark photons [5–8], and light fermions [9–11]. One broad category are *light relics*, stable particles which were in thermal contact with the SM in the early universe and decoupled while relativistic. Consequently, their cosmic abundance was frozen and survived until today. The quintessential example within the SM are neutrinos, but they need not be the only light relics to populate our universe. Different proposed new light relics include a fourth, sterile neutrino, whose existence is suggested by different anomalous experimental results [12–14] (see Ref. [15] for a recent review); as well as the gravitino, the supersymmetric partner of the graviton [16].

New relics that are sufficiently light will manifest as dark radiation, and can be searched for through their effect on the cosmic microwave background (CMB) anisotropies [17–19], typically parametrized by the effective number of neutrino species,  $N_{\text{eff}}$  (which is 3.045 in the standard cosmological model [20, 21]). Massive relics can, on the other hand, become non-relativistic at some point in cosmic history, and behave as dark matter (DM)

thereafter. However, their decoupling while relativistic gives these relics significant streaming motion, which sets a scale below which they cannot cluster, thus altering the large-scale structure (LSS) of our universe. This has allowed cosmology to set the leading constraints on neutrino mass, at  $\Sigma m_\nu < 0.26$  eV (95% C.L.), assuming standard cosmology [22]. In this work we will search for new Light—but Massive—Relics (LiMRs) using cosmological observables.

Cosmological data from near-future surveys are expected to provide exquisite measurements of the distribution of matter in our universe. LiMRs that have become non-relativistic before today (with masses  $m_X \gtrsim 1$  meV), will impact that distribution by behaving as hot DM [23–27]. In addition to the relic mass, two relevant parameters determine the relic abundance. The first is their number  $g_X$  of degrees of freedom. The second is their temperature  $T_X^{(0)}$  today. Due to comoving-entropy conservation, any relic that was in equilibrium with the SM in the early universe ought to have  $T_X^{(0)} \geq 0.91$  K. This minimum temperature gives rise to different values of  $\Delta N_{\text{eff}}$  for each type of relic [28]: 0.027 for scalars ( $g_X = 1$ ), 0.047 for Weyl fermions ( $g_X = 2$ ), 0.054 for massless gauge bosons ( $g_X = 2$ ), and 0.095 for Dirac fermions ( $g_X = 4$ ). In addition, relics with masses in the eV-scale will become non-relativistic before today, leaving an imprint in the form of suppressed matter fluctuations. Here we forecast how well eV-scale LiMRs can be observed by joint CMB and LSS surveys.

This paper is structured as follows. In Section II we briefly review light relics and their effects on cosmological observables. In Section III we detail the datasets we consider, which we employ in Section IV to forecast constraints on LiMRs within the mass range 10 meV-10 eV. We conclude in Section V.

## II. LIGHT RELICS AND THEIR EFFECT ON COSMOLOGICAL OBSERVABLES

We begin with an overview of the physics of light relics and their effects on cosmological observables. A LiMR  $X$  is characterized by its present-day temperature  $T_X^{(0)}$  and mass  $m_X$ , as well as its statistics, bosonic or fermionic, and its number  $g_X$  of degrees of freedom. The present-day temperature of a light relic (massive or not) is set by the time at which it decouples from the SM thermal bath, which is found as

$$T_X^{(0)} = \left( \frac{g_{*S}^{(0)}}{g_{*S}^{(\text{dec})}} \right)^{1/3} T_\gamma^{(0)}, \quad (1)$$

where  $g_{*S}^{(0/\text{dec})}$  denotes the entropy degrees of freedom in the universe today/when the relic decoupled, and  $T_\gamma^{(0)} = 2.725$  K is the present-day temperature of the photon bath. In this way, the conservation of comoving entropy provides a minimal light relic temperature assuming the SM with no additional degrees of freedom (other than the relic),

$$T_X^{(0)} \gtrsim \left( \frac{3.91}{106.75} \right)^{1/3} T_\gamma^{(0)} \approx 0.91 \text{ K}, \quad (2)$$

where just after the electroweak phase transition we have  $g_{*S}^{(\text{dec})} = 106.75$  encompasses all the known degrees of freedom of the Standard Model, and the present-day value of  $g_{*S}^{(0)} = 3.91$  includes photons and decoupled, cooler neutrinos. As an example, the SM (active) neutrinos have  $T_\nu^{(0)} = 1.95$  K, as they decoupled just prior to electron-positron annihilation where  $g_{*S}^{(\text{dec}, \nu)} = 10.75$ . Note that the baryonic and cold-dark matter (CDM) contributions are negligible, given their exponentially suppressed abundance.

In contrast, light relics decoupled while relativistic, and so are cosmologically abundant, with number densities comparable to that of photons or neutrinos. For instance, a Weyl fermion decoupling as early as possible (with minimal present-day temperature 0.91 K) will have a number density today of  $11 \text{ cm}^{-3}$ , and a vector boson that decouples just before  $e^+e^-$  annihilation (with a temperature today of 1.95 K, as neutrinos) will have a present-day number density of  $150 \text{ cm}^{-3}$ . Thus, the contribution of light relics to the cosmic energy budget can be significant.

It is often enlightening to describe the cosmological effects of other relics in relation to those of neutrinos, given their common origin as light relics. As advanced in the introduction, relics in the early universe (while  $T_X \gg m_X$ ) behave as radiation, and their cosmological impact while relativistic can be encapsulated in the number of effective neutrinos,  $N_{\text{eff}}$ , defined with respect to their contribution

to the radiation energy density,

$$\begin{aligned} \rho_{\text{rad}}(z) &= \frac{\pi^2}{30} \left( \sum_{\text{bosons}} g_b T_b^4(z) + \frac{7}{8} \sum_{\text{fermions}} g_f T_f^4(z) \right) \\ &\equiv \frac{\pi^2}{30} \left( 2T_\gamma^4(z) + \frac{7}{4} N_{\text{eff}} T_\nu^4(z) \right), \end{aligned} \quad (3)$$

where  $T_{\gamma/\nu}(z)$  is the temperature of photons and neutrinos at redshift  $z$ ,  $g_b/g_f$  are the degrees of freedom, and  $T_b/T_f$  are the temperatures of each boson/fermion, respectively.

Introducing an entropically significant light relic will generate a contribution to Eq. (3) of  $(\pi^2/30)g_X T_X^4$  for bosonic species, or  $7/8$  times that for fermionic species. We can then describe any departure from the predicted value of  $N_{\text{eff}}^{\Lambda\text{CDM}} = 3.045$  in the standard  $\Lambda\text{CDM}$  model by the quantity  $\Delta N_{\text{eff}}$ , given by

$$\Delta N_{\text{eff}} = c_1^\gamma \left( \frac{g_X}{g_\nu} \right) \left( \frac{T_X^{(0)}}{T_\nu^{(0)}} \right)^4, \quad (4)$$

in terms of the neutrino parameters  $g_\nu = 2$  and  $T_\nu^{(0)} = 1.95$  K. The factor  $c_1 = 8/7$  accounts for the difference between the Bose-Einstein ( $\gamma = 1$ ) and Fermi-Dirac ( $\gamma = 0$ ) distributions.

This discussion is encapsulated in Fig. 1, showing the relation between the present-day relic temperature to the time of relic decoupling, and its corresponding contribution to  $N_{\text{eff}}$ . Note that the present-day temperature of a relic for fixed decoupling epoch does not depend on particle species, but its contribution to radiation energy does.

Current limits on  $\Delta N_{\text{eff}}$  arise primarily from observables at two epochs. The first is recombination. Measurements of radiation at recombination are sensitive to relics lighter than  $\sim 0.1$  eV. The *Planck* 2018 analysis reports a measurement of  $N_{\text{eff}} = 2.99_{-0.33}^{+0.34}$  (TT+TE+EE+lowE+lensing+BAO) at 95% C.L. [22]. The proposed CMB-Stage 4 (CMB-S4) experiment is expected to refine this measurement to the  $\sigma(N_{\text{eff}}) = 0.03$  level [29]. The second is the Helium abundance, from where we can infer the number of relativistic species present during big bang nucleosynthesis (BBN). The 68% C.L. measurement during that era is  $N_{\text{eff}} = 2.85 \pm 0.28$  [30], which is valid for all relics lighter than  $m_X \lesssim 1$  MeV. Note that this does not affect dark matter produced via the freeze-in mechanism, as it can contribute negligibly to  $N_{\text{eff}}$  [31, 32].

In this work we consider detection prospects for four types of LiMRs: scalars, vectors, and both Dirac and Weyl fermions. We study relics with eV-scale masses,  $10 \text{ meV} \leq m_X \leq 10 \text{ eV}$ , such that they all behave as matter today, with the highest mass candidates constituting up to  $\sim 10\%$  of DM abundance. Finally, we also consider a range of temperatures, bounded by  $T_X^{(0)} \geq 0.91$  K from below. Our maximum temperature is informed by the constraint  $\Delta N_{\text{eff}} \leq 0.36$  from *Planck*, corresponding to a

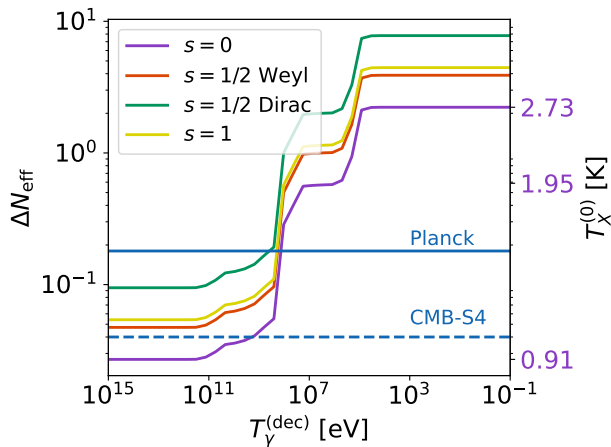


**FIG. 1:** Cosmic evolution of  $\Delta N_{\text{eff}}$  due to a light relic that decoupled when the universe had a temperature  $T_{\gamma}^{(\text{dec})}$ . We assume four different types of relics with spin  $s$ , as described in the text, and show the 68% C.L. constraints achieved by *Planck* as a horizontal solid line, and the forecast by CMB-S4 in dashed lines. The right vertical axis shows what the temperature of the relic would be today, following the violet (lowest) curve plotted for  $s = 0$ . Note that these constraints only apply to relics with  $m_X \approx 0.1$  eV or lighter.

single additional species of Weyl fermion at  $T_X^{(0)} \leq 1.5$  K. This bound could be further improved by combining with BBN measurements of e.g. D/H ratios [33], Lyman- $\alpha$  forest flux power spectrum data [34, 35], as well as Baryon Acoustic Oscillations (BAO) and galaxy power spectrum measurements [36–38].

### Effect on the LSS of the Universe

LiMRs can become non-relativistic at some point in cosmic history, and comprise a fraction of DM today. Unlike CDM, which is expected to compose the majority of the matter sector, LiMRs have significant thermal motions, even if non-relativistic. Thus, these relics will stream away from structures below their free-streaming scale, which during matter domination is given by [39, 40]

$$k_{\text{fs}} = \frac{0.08}{\sqrt{1+z}} \left( \frac{m_X}{0.1 \text{ eV}} \right) \left( \frac{T_X^{(0)}}{T_{\nu}^{(0)}} \right)^{-1} h \text{ Mpc}^{-1}. \quad (5)$$

Throughout this section we assume a Weyl fermionic relic, and we will relax this assumption later. This presents another way of searching for LiMRs: through their effect on the matter fluctuations. LiMRs produce a suppression in the matter power spectrum at scales smaller than  $k_{\text{fs}}$ , which we discuss below. The size of this suppression depends on the present abundance of

the LiMR, which (if non-relativistic) is given by

$$\Omega_X h^2 = \frac{m_X}{93.14 \text{ eV}} \frac{g_X}{g_{\nu}} \left( \frac{T_X^{(0)}}{T_{\nu}^{(0)}} \right)^3. \quad (6)$$

From Eq. (6) we see that there is a maximum allowed particle mass, found by saturating the observed DM abundance  $\Omega_{\text{cdm}} h^2 = 0.12$  [22]. For a relic temperature  $T_X^{(0)} \approx 1.5$  K, this is  $m_X \approx 10$  eV. Additionally, in this work we are interested in the relics that become non-relativistic before today. Thus, the mass range we will study encompasses

$$10 \text{ meV} \leq m_X \leq 10 \text{ eV}. \quad (7)$$

LiMRs produce a suppression in matter fluctuations, similar to neutrinos, due to two reasons. The first is simply that the light relic does not cluster at small scales, and its fluctuation  $\delta_X$  at small-scale roughly follows  $\delta_X = (k/k_{\text{fs}})^{-2} \delta_m$  with respect to the matter overdensity  $\delta_m$ . The second is that the absence of relic fluctuations at small scales slows down the growth of CDM (and baryon) overdensities. Together, these two factors produce a suppression of roughly  $(1 - 14 f_X)$  in the matter power spectrum [41], where  $f_X$  is the fraction of matter that is composed of the LiMR  $X$ . This suppression is less pronounced for relics that stay relativistic for longer, which yields the well-known result of  $(1 - 8 f_{\nu})$  for neutrinos comprising a fraction  $f_{\nu}$  of matter, as neutrinos only become non-relativistic during matter domination. These numbers are for illustration purposes only, and in all cases we find the full effect of LiMRs on the cosmological observables using the publicly available software CLASS [42]. Nevertheless, they provide intuition about the physical effect of such a relic. While the mechanism that produces the suppression is the same as for neutrino masses, the free-streaming scale  $k_{\text{fs}}$  for a LiMR is not fully determined by its mass (or abundance), as their temperature today is unknown. Relics that are still relativistic today (with  $m_X \lesssim \text{meV}$ ) will have never collapsed into structures and thus their observable effects can be fully included into  $\Delta N_{\text{eff}}$ . In practice, this is the case for LiMRs with masses below  $\sim 0.1$  eV, as we will show, so we will use our results for a 10 meV relic for lighter masses.

To study LiMRs, the relevant observables are the fluctuations of baryons and cold dark matter, as only those will gravitationally bind to form the visible structures we observe as galaxies, the relics being too light to cluster (see, however, Ref. [43]). The power spectrum of baryonic plus cold dark-matter fluctuations is modeled by

$$P_{\text{cb}}(k) = P_{\zeta}(k) \left( f_b T_b + f_c T_c \right)^2, \quad (8)$$

where  $P_{\zeta}$  is the primordial power spectrum, the transfer functions  $T_b$  and  $T_c$  are found using CLASS [42], and the fractional abundances are defined by

$$f_{b/c} \equiv \frac{\omega_{b/c}}{\omega_b + \omega_c}, \quad (9)$$

where  $\omega_b$  and  $\omega_c$  are the baryon and CDM abundances.

We show the suppression in  $P_{cb}$  in Fig. 2 (upper panel) for a fermion with  $m_X = 0.02$  eV and  $T_X = 0.91$  K, for degrees of freedom  $g_X = 2, 3$  and 4. In all cases the high- $k$  power is more suppressed, as expected. Increasing the abundance of the LiMR, by augmenting  $g_X$ , produces a more marked suppression, while keeping the shape fixed. Moreover, increasing the relic abundance produces wiggles at the BAO scale, as the LiMR both contributes as radiation at recombination and free streams – like neutrinos – changing the BAO phase [17].

The suppression of matter fluctuations produces a change in the biasing of galaxies, which has been calculated for both neutrinos and other relics [44–46], and accounted for in neutrino-mass forecasts in our companion paper [47]. This produces a growth in the galaxy power spectrum that partially compensates the relic-induced suppression. Here we account for this growth induced scale-dependent bias (GISDB) by multiplying the Lagrangian bias by a  $k$ -dependent factor

$$g(k) = R_L^{\Lambda\text{CDM}}(k) R_L^X(k) R_L^\nu(k), \quad (10)$$

where the functions  $R_L^i$  account for different effects, following Ref. [45]. First,  $R_L^{\Lambda\text{CDM}}$  accounts for the step-like change in the growth rate of fluctuations before and after matter-radiation equality, parametrized as

$$R_L^{\Lambda\text{CDM}}(k) = 1 + \Delta_{\Lambda\text{CDM}} \tanh\left(\frac{\alpha k}{k_{\text{eq}}}\right), \quad (11)$$

where  $\Delta_{\Lambda\text{CDM}} = 4.8 \times 10^{-3}$  and  $\alpha = 4$  determine the amplitude and location of the step, given the scale  $k_{\text{eq}}$  of matter-radiation equality. The two other factors account for the effect of a LiMR on the matter power spectrum, also taken to be a step-like function

$$R_L^i(k) = 1 + \Delta_i \tanh\left(1 + \frac{\ln q_i(k)}{\Delta q}\right), \quad (12)$$

with an amplitude  $\Delta_i = 0.6 f_i$  determined by the fraction  $f_i$  of matter composed of the relic  $i$  ( $X$  or  $\nu$ ), width  $\Delta q = 1.6$ , and where we have defined  $q_i(k) \equiv 5k/k_{\text{fs},i}$ , given the free-streaming scale  $k_{\text{fs},i}$  of each LiMR.

### Effect on the CMB

The CMB is sensitive to the presence of LiMRs in the universe, through their mean energy density [48, 49] and their perturbations [50, 51]. Their additional energy density changes the expansion rate of the universe, which in turn affects the CMB damping tail. Since matter-radiation equality is very well measured through the location of the first acoustic peak, this causes the power spectrum to be suppressed on short-wavelength modes. In addition to this effect, their perturbations cause a change in the amplitude and a shift in the location of the CMB acoustic peaks (for a review of the phase shift in the acoustic peaks in the CMB, see Ref. [19]).

We show an example of the effect of a LiMR on the CMB in Fig. 2 – again for a fermion with  $m_X = 0.02$  eV and  $T_X = 0.91$  K, for degrees of freedom  $g_X = 2, 3$  and 4. The amplitude and phase shift of the BAO is clearly seen to increase with  $g_X$ .

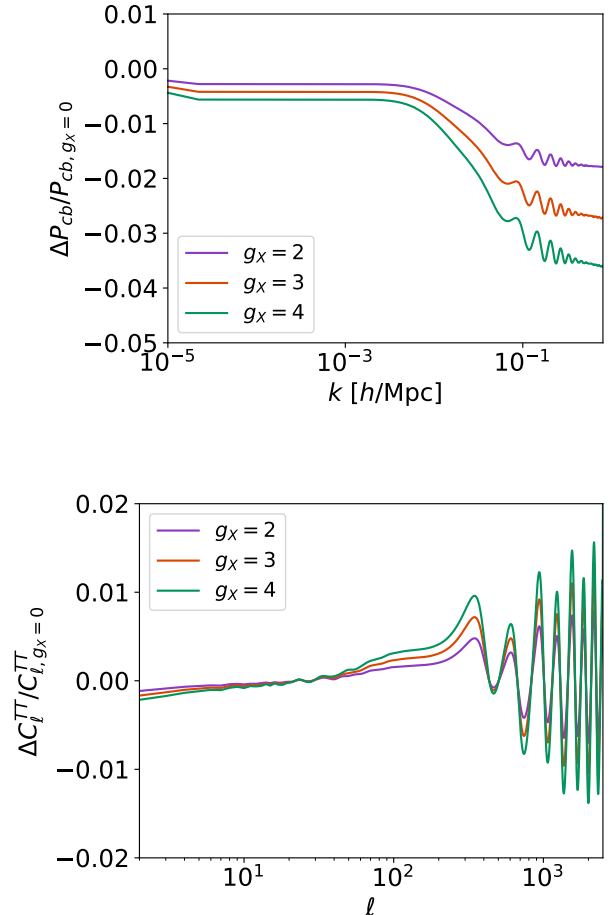


**FIG. 2:** Effect of introducing a fermion with degrees of freedom  $g_X$ , temperature  $T_X = 0.91$  K and mass  $m_X = 0.02$  eV on the CDM+baryon power spectrum (upper panel) and the CMB temperature power spectrum (lower panel). Here all cosmological parameters are fixed when introducing the LiMR. We note that an effective fractional number of degrees of freedom may be achieved as a result of out-of-equilibrium processes.

### Types of Relic

Throughout this work we will study four major types of LiMRs, two fermionic and two bosonic, which we now describe.

In the fermionic category, the first type we study are the neutrino-like Weyl fermions, with non-zero mass, spin  $s = 1/2$ , and two degrees of freedom ( $g_X = 2$ ). In ad-



dition to sterile neutrinos, an intriguing example is the gravitino, the supersymmetric partner of the graviton. While the gravitino has  $s = 3/2$ , only the longitudinal modes couple to the Standard Model and hence behaves equivalently to an  $s = 1/2$  particle with  $g_X = 2$ . The gravitino is predicted in models of supersymmetric gravity to have a mass in the eV range [52, 53], within the range relevant to our study. The second type we tackle are the related Dirac fermions, such as the axino [54], which simply have twice as many degrees of freedom ( $g_X = 4$ ).

In the bosonic category we study two types of particles as well: firstly scalars, with only one degree of freedom ( $g_X = 1$ ). A realization of this model could be a Goldstone boson, which can have naturally small masses. The second type are spin-1 vectors. We assume that they have a Stueckelberg mass, as it is technically natural [55] and avoids complications from Higgs mechanisms. While this relic will be non-relativistic today, its longitudinal mode was decoupled in the early universe (while it was relativistic), and thus only two of the three degrees of freedom were populated. Therefore, this relic has  $g_X = 2$ .

Instead of modifying the distribution function for each type of relic, we will take advantage of the fact that any relic, whether bosonic or fermionic, can be recast onto an equivalent Weyl relic (i.e., a neutrino with  $g_W = 2$ ), with some temperature  $T_W^{\text{eq}}$  and mass  $m_W^{\text{eq}}$  [23, 45]. Assuming a relic of temperature  $T_X$ , with  $g_X$  degrees of freedom, the equivalent Weyl relic has

$$T_W^{\text{eq}} = T_X (g_X/g_W)^{1/4} c_1^{\gamma/4} \quad (13)$$

$$m_W^{\text{eq}} = m_X (g_X/g_W)^{1/4} c_1^{\gamma/4} c_2^{\gamma}, \quad (14)$$

where we correct for the different distributions of these particles by setting  $\gamma = 1$  for bosons (and  $\gamma = 0$  for our base case of fermions as before), with constants  $c_1 = 8/7$  (as in Eq. 4) and  $c_2 = 7/6$ . Note that our normalization is slightly different from that found in Ref. [45], as there fermionic degrees of freedom contributed by  $3/2$ .

### III. METHODS

We now present our forecasting methods. In this first exploratory work we will follow a Fisher-matrix approach, in order to efficiently explore the 2D parameter space  $(T_X^{(0)}, m_X)$  of possible LiMRs. We encourage the reader to visit Appendix A for a comparison against MCMC results. We will also cover different combinations of datasets. For the CMB, we will study the current *Planck* satellite [22] as well as the upcoming ground-based CMB-S4 [56]. On the galaxy-survey side we will consider the current BOSS [57], the ongoing DESI [58], and the upcoming *Euclid* [59] surveys.

#### A. Parameters

We are interested in forecasting how well different LiMRs with varied temperatures and masses can be detected. Therefore, a simple Fisher forecast of the relic mass and temperature, assuming a particular fiducial relic, is insufficient. Instead, we will find how well LiMRs of varying mass  $m_X$  and temperature  $T_X^{(0)}$  can be observed by different experiments. The parameter we will forecast is  $g_X$ , the number of degrees of freedom of the LiMR.<sup>1</sup> Then,  $g_X/\sigma(g_X)$  is a good proxy for the significance at which a LiMR of a particular  $m_X$  and  $T_X^{(0)}$  can be detected.

In order to properly search for a LiMR we have to marginalize over the six  $\Lambda$ CDM parameters. These include the baryon and cold dark-matter abundances,  $\omega_b$  and  $\omega_{\text{cdm}}$  (with fiducial values of  $\omega_b = 0.02226$  and  $\omega_{\text{cdm}} = 0.1127$ ), the (reduced) Hubble constant  $h = 0.701$ , and the optical depth  $\tau_{\text{reio}} = 0.0598$  to reionization. The last two parameters are the amplitude  $A_s$ , and tilt  $n_s$ , of primordial fluctuations, with fiducial values of  $A_s = 2.2321 \times 10^{-9}$  and  $n_s = 0.967$ . In addition, we marginalize over the effect of neutrino masses. We assume for our fiducial model the existence of three degenerate massive neutrinos, with  $\sum m_\nu = 0.06$  eV, and we will report constraints both with and without marginalization over neutrino masses. For a discussion about the effect of the neutrino hierarchy see Refs. [47, 60].

#### B. CMB experiments

We will model both *Planck* and CMB-S4 as having a single effective observing frequency, to avoid marginalizing over foregrounds. For *Planck* we will use CMB temperature ( $T$ ) and  $E$ -mode polarization data, covering the range  $\ell = [2 - 2500]$ . We take noises of  $\Delta_T = 43 \mu\text{K-arcmin}$  and  $\Delta_E = 81 \mu\text{K-arcmin}$ , with a  $\theta_{\text{FWHM}} = 5$  arcmin angular resolution. This well approximates the (more complex) *Planck* data likelihood.

For CMB-S4 we take  $\Delta_T = 1 \mu\text{K-arcmin}$ , and  $\Delta_E = \sqrt{2} \Delta_T$ , with an angular resolution of  $\theta_{\text{FWHM}} = 3$  arcmin. Additionally, we include lensing data, where we perform iterative delensing of  $B$ -modes to lower the noise, as in Refs. [61, 62]. All modes cover the range  $\ell = [30 - 5000]$ , except for the  $TT$  autocorrelation, where we do not go beyond  $\ell = 3000$  to avoid foreground contamination [29]. We add a Gaussian prior on the optical depth of reionization of  $\sigma(\tau_{\text{reio}}) = 0.01$ , instead of the  $\ell < 30$  modes in this case. This follows the prescription in the CMB-S4 Science Book [29], as well as our companion paper [47].

<sup>1</sup> We note that, while  $g_X$  appears to be a fixed quantity for a given relic, e.g.  $g_X = 1$  for a scalar, changing  $g_X$  simply means altering the amount of relic particles (as both  $\Delta N_{\text{eff}} \propto g_X$  and  $\Omega_X \propto g_X$ ) while keeping their thermal properties identical. That makes  $g_X$  a useful variable to forecast.

The CMB data will perform two main roles. First, it will very precisely measure the standard cosmological parameters, breaking many degeneracies in the LSS data. Second, the CMB is sensitive to the effects of a LiMR both during recombination and in the matter fluctuations at lower redshifts, through the weak lensing information.

### C. Galaxy surveys

For the LSS data we will consider three surveys, all of them spectroscopic. We leave for future work studying the promise of photometric surveys, such as the Vera Rubin Observatory [63], and weak-lensing surveys, such as the Dark Energy Survey [64].

We take the luminous red galaxy (LRG) sample of the Sloan Digital Sky Survey Baryon Oscillation Spectroscopic Survey (BOSS) [57], which will serve as an indication of the power of current data. To showcase the promise of upcoming surveys we study the emission-line galaxy (ELG) sample of the Dark Energy Spectroscopic Instrument (DESI) [58], and the more futuristic H $\alpha$ -emitters of *Euclid* [59]. We restrict our analysis to a single tracer, the most populous for each survey, though more optimistic results are expected for multi-tracer approaches [65]. The noise per redshift bin for each sample is reported in Table I. We assume sky coverages of 10,000 deg<sup>2</sup> for BOSS; 14,000 deg<sup>2</sup> for DESI; and 15,000 deg<sup>2</sup> for *Euclid*.

As each of these surveys contain distinct tracers, the bias description of each will be somewhat different as well. Here we follow a simple approach, and parametrize the linear Eulerian bias as

$$b_1(k, z) = [1 + b_L(k, z) + \alpha_{k2}k^2], \quad (15)$$

where the  $\alpha_{k2}$  term (with a fiducial value of 1 Mpc<sup>2</sup>) accounts for non-linearities in the bias [66]. An additional scale-dependence comes from the aforementioned GISDB effect, which enters in the Lagrangian bias,

$$b_L(k, z) = [b_0(z) - 1]g(k), \quad (16)$$

where  $g(k)$  is as defined in Eq. (10). The redshift evolution of the bias is encapsulated in the term  $b_0(z)$ , which is chosen such that the scale-independent (i.e.,  $k \rightarrow 0$ ) behavior of the Eulerian bias matches with simulations for the tracer in question. For the ELGs in DESI we match to

$$b_0(z) = \frac{\beta_0}{D(z)}, \quad (17)$$

where  $D(z)$  is the growth factor and  $\beta_0 = 1$  [58]; whereas for the tracers in BOSS and *Euclid* we take

$$b_0(z) = \beta_0(1+z)^{0.5\beta_1}, \quad (18)$$

with fiducials  $\beta_0 = 1.7$  and  $\beta_1 = 1$  as in Ref. [67]. We marginalize over the nuisance parameters  $\beta_0$ ,  $\alpha_{k2}$ , as well

as  $\beta_1$  for BOSS and *Euclid*. We note that a full analysis of the data might require marginalization over the amplitude of the bias at each redshift bin independently, which would however lead to a loss in constraining power.

### D. Fisher matrix

We will obtain forecasted constraints using the Fisher-matrix formalism [69–71]. For the CMB we follow the approach of Refs. [72, 73]. For the galaxy observables we detail below how we construct our Fisher matrix.

As described in Section II, LiMRs suppress the clustering of matter in our universe, and as a consequence, that of biased tracers of matter, such as galaxies. We take into account several effects to convert from matter to galaxy fluctuations. First, there are redshift-space distortions (RSD), induced by the gravitational infall into, and peculiar velocities of galaxies [74, 75]. We write the galaxy power spectrum as

$$P_g(k, \mu) = \mathcal{R}(k, \mu)\mathcal{F}(k, \mu)P_{cb}(k), \quad (19)$$

in terms of the power spectrum  $P_{cb}(k)$  of CDM + baryon fluctuations, where the two pre-factors  $\mathcal{R}$  and  $\mathcal{F}$  account for the RSD and the finger-of-god (FoG) effect, both of which make  $P_g$  anisotropic, as they depend on  $\mu = \hat{k} \cdot \hat{n}$ , the line-of-sight angle.

We model the linear RSD term simply as

$$\mathcal{R}(k, \mu) = [b_1(k) + f\mu^2]^2, \quad (20)$$

where  $b_1$  is the linear Eulerian bias, as described above, and  $f \equiv d \ln D / d \ln a$  is the logarithmic derivative of the growth factor  $D$ , which can be well approximated by [76]

$$f(z) = \left( \frac{\Omega_M(1+z)^3}{\Omega_M(1+z)^3 + \Omega_\Lambda} \right)^\gamma, \quad (21)$$

with  $\gamma = 0.55$ . The non-linear FoG effect is included in the term

$$\mathcal{F}(k, \mu) = \exp[-k^2\mu^2\sigma_v^2/H^2], \quad (22)$$

with  $\sigma_v = (1+z)\sqrt{c^2\sigma_z^2 + \sigma_{\text{FoG}}^2}/2$ , where  $\sigma_{\text{FoG}} = \sigma_{\text{FoG}}^{(0)}\sqrt{1+z}$ , with  $\sigma_{\text{FoG}}^{(0)} \equiv 250 \text{ km s}^{-1}$  [77] as the intrinsic velocity dispersion of galaxies, and we take a spectroscopic redshift error  $\sigma_z \equiv 0.001c$  [58], which corresponds to the DESI precision requirement at  $z = 1$ .

In addition, we include the Alcock-Paczynski (AP) effect [78–80], which accounts for changes in the observed  $k$  and  $\mu$  and the comoving volumes from assuming different cosmologies. For that, we write the observed galaxy power spectrum as [81]

$$\tilde{P}_g(k', \mu') = P_g(k, \mu) \left( \frac{H_{\text{true}}}{H_{\text{fid}}} \right) \left( \frac{D_{A,\text{fid}}}{D_{A,\text{true}}} \right)^2, \quad (23)$$

where the subscript “fid” refers to fiducial, and the “true” wavenumber  $k'$  and angle  $\mu'$  are given by

$z$	0.05	0.15	0.25	0.35	0.45	0.55	0.65	0.75	0.85	0.95
$\frac{dN_{LRG}}{dz \, d\text{deg}^2}$ [BOSS]	8	50	125	222	332	447	208	30	0	0
$\frac{dN_{ELG}}{dz \, d\text{deg}^2}$ [DESI]	0	0	0	0	0	0	309	2269	1923	2094
$\frac{dN_{H\alpha}}{dz \, d\text{deg}^2}$ [ <i>Euclid</i> ]	0	0	0	0	0	0	2434.28	4364.81	4728.56	4825.80

$z$	1.05	1.15	1.25	1.35	1.45	1.55	1.65	1.75	1.85	1.95
$\frac{dN_{LRG}}{dz \, d\text{deg}^2}$ [BOSS]	0	0	0	0	0	0	0	0	0	0
$\frac{dN_{ELG}}{dz \, d\text{deg}^2}$ [DESI]	1441	1353	1337	523	466	329	126	0	0	0
$\frac{dN_{H\alpha}}{dz \, d\text{deg}^2}$ [ <i>Euclid</i> ]	4728.80	4507.63	4269.85	3720.66	3104.31	2308.98	1514.83	1474.71	893.72	497.61

**TABLE I:** Forecasted number of target galaxies measurable by each survey: LRGs for BOSS, ELGs for DESI, and H $\alpha$  emitters for *Euclid* per redshift per deg<sup>2</sup> at each redshift bin  $z$ , taken from Refs. [58, 59, 68].

$$k' = k \left[ (1 - \mu^2) \frac{D_{A,\text{fid}}^2(z)}{D_{A,\text{true}}^2(z)} + \mu^2 \frac{H_{\text{true}}^2(z)}{H_{\text{fid}}^2(z)} \right]^{1/2} \quad (24)$$

$$\mu' = \mu \frac{k}{k'} \frac{H_{\text{true}}(z)}{H_{\text{fid}}(z)}. \quad (25)$$

Properly accounting for the AP effect, thus, implies evaluating the entire galaxy power spectrum at different wavenumbers for each cosmological-parameter change. That can be computationally consuming, so instead we will perform a simpler step that is accurate to first order in derivatives (as any further is not captured by Fisher). Therefore, we can write

$$\frac{\partial \tilde{P}_g(k', \mu')}{\partial \theta_i} = \frac{\partial P_g(k, \mu)}{\partial \theta_i} + \mathcal{C}_i(k), \quad (26)$$

for each parameter  $\theta_i$ , where

$$\mathcal{C}_i(k) = \frac{\partial P_g}{\partial k} \frac{dk}{d\theta_i} + \frac{\partial P_g}{\partial \mu} \frac{d\mu}{d\theta_i}, \quad (27)$$

accounts for the AP correction to linear order, with the derivatives of  $k$  and  $\mu$  computed from Eq. (25).

The Fisher element for parameters  $\theta_i, \theta_j$  is then calculated as [68]

$$F_{ij} = \sum_z \int k^2 dk \int d\mu \frac{V(z)}{2(2\pi)^2} \left( \frac{\bar{n} \tilde{P}_g}{\bar{n} \tilde{P}_g + 1} \right)^2 \left( \frac{\partial \log \tilde{P}_g}{\partial \theta_i} \right) \left( \frac{\partial \log \tilde{P}_g}{\partial \theta_j} \right), \quad (28)$$

where  $V(z)$  is the comoving volume for each redshift bin summed over, and  $\bar{n}(z)$  is the comoving number density of tracers, given by  $\bar{n}(z) =$

$\Delta z f_{\text{sky}} V^{-1}(z) dN / (dz \, d\text{deg}^2)$ , where the last factor is reported for each survey in Table I. The integral over  $\mu$  goes from  $-1$  to  $1$ , and over wavenumbers from  $k_{\text{min}} = \pi V(z)^{-1/3}$  to  $k_{\text{max}} = 0.2h \, \text{Mpc}^{-1}$ . While at higher  $z$  the fluctuations are smaller and, thus, we could reach higher  $k_{\text{max}}$  while linear, the biasing of galaxies becomes more complicated, so we fix it for all  $z$ .

## IV. RESULTS

In this section we discuss our cosmological constraints for a LiMR. We will perform two parallel analyses. First, we will show the reach of different combinations of datasets by forecasting  $\sigma(g_X)$  for a Weyl (neutrino-like) relic of different masses and temperatures, covering the entire range of interest. Then, we will focus on the minimal case (that with  $T_X^{(0)} = 0.91 \, \text{K}$ ) for the four relic types we consider, and find more precisely above which mass  $m_X$  they can be ruled out.

### A. Full Parameter Space

We will start with a Weyl relic, and cover a broad range of cases, where in each case we will assume that there exists a LiMR in our universe with mass  $m_X$  and temperature today  $T_X^{(0)}$ , and forecast how well  $g_X$  can be measured as a measure of how significant a detection would be.

We scan through a range of LiMR masses  $m_X$  from  $10^{-2} \, \text{eV}$ , as all lighter relics behave identically, up to  $\sim 10 \, \text{eV}$ , where the relic abundance overcomes that of all DM. As for their temperature, we cover  $T_X^{(0)} = [0.91 - 1.50]$

K, where the lower limit is as found in Section II, and the upper limit saturates the current 95% C.L. *Planck* + BOSS DR12 BAO limit on  $N_{\text{eff}}$  [22].

First, as a test, we forecast the errors on  $N_{\text{eff}}$  by looking at our lightest relic ( $m_X = 0.01$  eV) as a proxy of the massless case, and translating the forecasted error  $\sigma(g_X)$  in the degrees of freedom into

$$\sigma(N_{\text{eff}}) = \frac{\sigma(g_X)}{g_\nu} \left( \frac{T_X^{(0)}}{T_\nu^{(0)}} \right)^4. \quad (29)$$

For reference, we have confirmed that assuming lower values of  $m_X$  result in the same forecasts for  $N_{\text{eff}}$ . This result is largely independent of the chosen  $T_X^{(0)}$ , so we will show forecasts for a Weyl fermion with  $T_X^{(0)} = 0.91$  K.

Beginning with the CMB, the *Planck*-only forecast gives  $\sigma(g_X) = 8.11$  corresponding to  $\sigma(N_{\text{eff}}) = 0.19$  which is in agreement with the *Planck* value of  $\sigma(N_{\text{eff}})$  in non-photon radiation density when allowing extra relativistic degrees of freedom Ref. [22]. Likewise, the CMB-S4-only forecast yields  $\sigma(N_{\text{eff}}) = 0.04$ , in agreement with Ref. [29]. In both cases, as well as the ones below, we account for a noted degeneracy with  $\Sigma m_\nu$  by marginalizing over the neutrino mass in our forecasts. Adding LSS data only improves these results, as we show in Table II. In particular, we find that adding BOSS to *Planck* gives  $\sigma(N_{\text{eff}}) = 0.14$ ; substituting DESI for BOSS yields  $\sigma(N_{\text{eff}}) = 0.06$ . Looking to the future, Euclid and CMB-S4 will lower this constraint to  $\sigma(N_{\text{eff}}) = 0.02$ .

We now move to non-zero masses, and provide marginalized posteriors from forecasts for a 0.91 K (minimum temperature) Weyl relic at different masses in Fig. 3. We only show the 2D contours between  $g_X$  and other cosmological parameters; for the full triangle plots at fixed mass  $m_X = 0.01$  eV, see Appendix B. The combination of information from the CMB and LSS can be seen to significantly improve constraints by breaking parameter degeneracies present in the individual datasets. Interestingly, the degeneracy directions change with LiMR mass. As an example, the degeneracy line for  $g_X$  and  $\omega_{\text{cdm}}$  for CMB data changes direction as the LiMR becomes more massive, and starts behaving as matter instead of radiation at recombination. The LSS degeneracy line, however, stays relatively stable, improving the CMB result by different amount at each mass.

The result described above indicates that combining CMB and LSS information is critical for an optimal constraint of LiMRs. We confirm this in Fig. 4, where we show the forecasted error in  $g_X$  for CMB and LSS data on their own, as well as together, which dramatically improves the constraints. For the rest of this work we will consider different combinations of CMB and LSS surveys together.

We now forecast to which level of significance different LiMR can be constrained, under three different survey combinations. The first is what would be realizable by current data, where we assume galaxy data from BOSS

and *Planck* for the CMB. We show the forecasted  $\sigma(g_X)$  in Fig. 5, which clearly shows that LiMRs with larger  $T_X^{(0)}$  and  $m_X$  are more readily observable. However, to observe (or rule out) a LiMR at  $3\sigma$  it has to be relatively heavy ( $m_X \gtrsim \text{few eV}$ ), as we will see below. Note that in this figure we show results for  $T_X^{(0)} < 0.91$  K, as for instance a scalar at that minimum temperature would be equivalent to a Weyl fermion with  $T_X^{(0)} = 0.79$  K, as we will discuss below.

The second case we consider is the near-future one, where we add DESI data to *Planck*. We show the forecasted constraints on  $g_X$  for this combination in Fig. 6, which are clearly improved with respect to the results shown in Fig. 5. In this case one can rule out relics of any mass with  $T_X^{(0)} = 1.4$  K at  $3\sigma$ . More interestingly, we see that masses above 1 eV would be ruled out, even for the lowest possible relic temperature of  $T_X^{(0)} = 0.91$  K.

The final case we consider is more futuristic, and adds CMB-S4 data to DESI. We show the results in Fig. 7, which further improves the prospects for detecting light relics. In this case even relics at low temperatures can be ruled out at  $3\sigma$  confidence for masses above 0.78 eV, whereas minimum-temperature massless Weyl relics can only be found at at  $0.5\sigma$  confidence.

## B. Minimum Temperature

While the figures discussed above covered a broad range of temperatures and masses, they all assumed a Weyl relic. Here we extend our results to other types of relics, focusing on the minimum temperature of  $T_X^{(0)} = 0.91$  K, corresponding to the earliest decoupling from the SM plasma. We divide our results into fermionic and bosonic relics. The cumulative results of our forecast for each type of particle are tabulated in Table III.

### Fermionic Relics

We start with a massive Weyl fermion with  $T_X^{(0)} = 0.91$  K, for which we show our forecasts on  $\sigma(g_X)$  for various combinations of galaxy surveys and CMB experiments in Fig. 8a, with a finer mass resolution than the results above. We report the minimum relic masses that are observable at  $3\sigma$  significance, both with (and without) marginalizing over the neutrino masses, as a test of how degenerate LiMRs are with the total neutrino mass. The combination of presently available *Planck* and BOSS datasets are forecasted to observe or rule out LiMRs above 2.85 (2.47) eV at  $3\sigma$  significance. For *Planck* and DESI, this is lowered to LiMRs with masses above 1.20 (1.00) eV. This result should motivate an analysis using presently available datasets. For the futuristic combination of CMB-S4 and *Euclid* datasets, we show that LiMR



$\sigma(N_{\text{eff}})$	CMB Only	BOSS	DESI	<i>Euclid</i>
LSS Only		0.92 (0.84)	0.29 (0.25)	0.20 (0.13)
<i>Planck</i>	0.19 (0.19)	0.14 (0.08)	0.06 (0.04)	0.06 (0.04)
CMB-S4	0.04 (0.04)	0.04 (0.03)	0.03 (0.02)	0.02 (0.02)

**TABLE II:** Forecasted  $1\sigma$  errors on  $N_{\text{eff}}$  from different combinations of experiments. Numbers in parenthesis assume fixed total neutrino mass, whereas the rest are marginalized over neutrino masses.

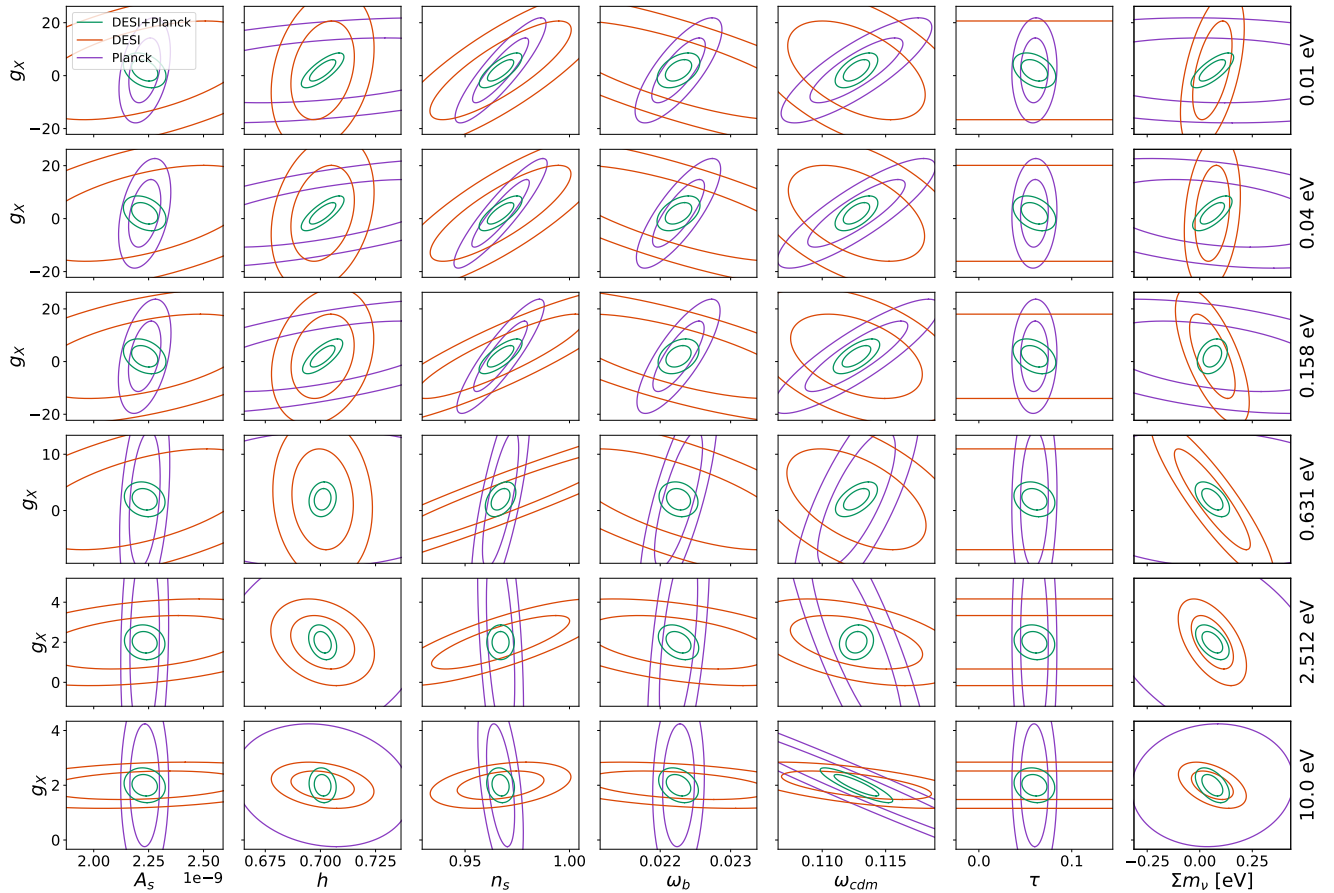


**FIG. 3:** 68% C.L. and 95% C.L. projected confidence ellipses for each of the parameters we marginalize over, as well as the LiMR number  $g_X$  of degrees of freedom, for DESI (red), *Planck* (purple), and their combination (green). Each row has a different fiducial relic mass, denoted on the right, all with an assumed temperature  $T_X^{(0)} = 0.91$  K today. Note that we also marginalize over the unknown neutrino mass, which loosens our constraints by as much as 143% for LSS-only information, 64% for CMB-only information, and 81% for combined LSS and CMB information.

masses above 0.63 (0.59) eV can be observed or ruled out at  $3\sigma$  significance.

As an example of the physical implications of these constraints, let us apply to them to the ( $s = 3/2$ ) gravitino, which is related to the scale of SUSY breaking in some models. The gravitino is cosmologically equivalent to the neutrino-like Weyl relic that we have studied, as only the  $s = 1/2$  modes are thermalized with the SM plasma in the early universe [52], and are expected to have the lowest relic temperature of 0.91 K. This has al-

lowed previous work to constrain the gravitino mass by requiring that their abundance does not overcome that of the cosmological dark matter [82]. Our forecast above shows that current data is sensitive to gravitinos heavier than  $m_X = 2.85$  eV, which is around the benchmark of some models of SUSY breaking [83, 84], and a factor of a few better than the best limits currently available [52, 85]. Upcoming data from CMB-S4 combined with *Euclid* is expected to further detect such gravitino population masses above 0.63 eV. Under the assumption

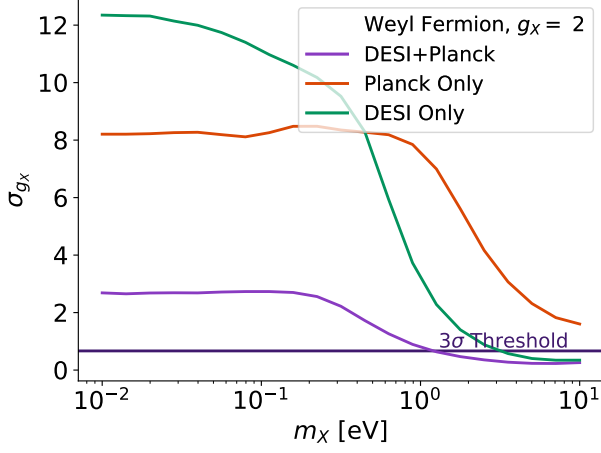


**FIG. 4:** Improvement of Weyl relic measurements by addition of LSS data with DESI and *Planck* constraints. As shown, the joint constraints are much stronger than the LSS or CMB alone.

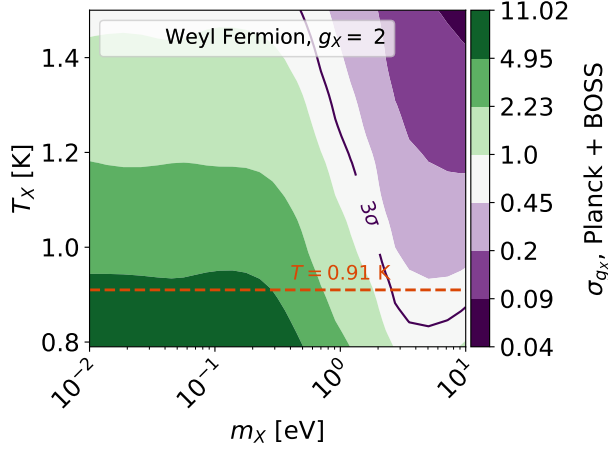


**FIG. 5:** Forecasted errors on  $g_X$  for a Weyl (neutrino-like) relic of different fiducial masses and temperatures, in all cases with fiducial  $g_X = 2$ , assuming BOSS+*Planck* data. The region of parameter space measurable at the  $3\sigma$ -level lays rightward of the purple solid line, and the dashed red line shows the minimum temperature expected for a relic.

that a cosmological gravitino population no longer exchanges entropy after decoupling from the SM bath, we can relate constraints on  $m_X$  to bounds on the SUSY breaking scale  $\Lambda_{\text{SUSY}} \sim \sqrt{m_X M_{\text{Pl}}}$  [53, 86]. Our forecasted *Planck* and BOSS dataset translates to an upper bound  $\Lambda_{\text{SUSY}} \lesssim 80$  TeV, whereas the CMB-S4 and *Euclid* datasets lower this to  $\Lambda_{\text{SUSY}} \lesssim 50$  TeV. These projections are interestingly complementary to the energy range that will be reached by the proposed  $\mathcal{O}(100 \text{ TeV})$  particle collider, showing the promise of our approach.

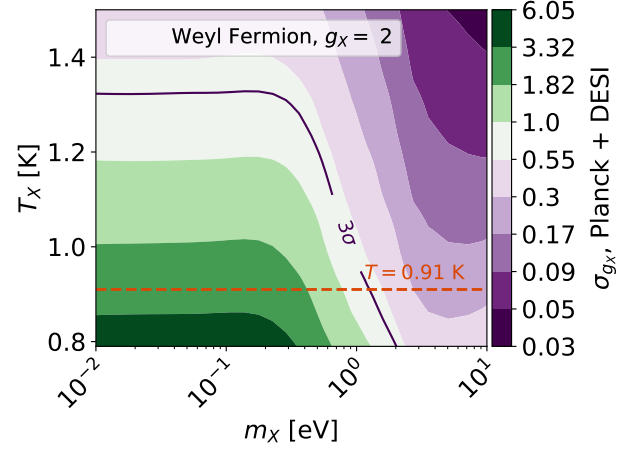


**FIG. 6:** Same as Fig. 5 for DESI + *Planck*.

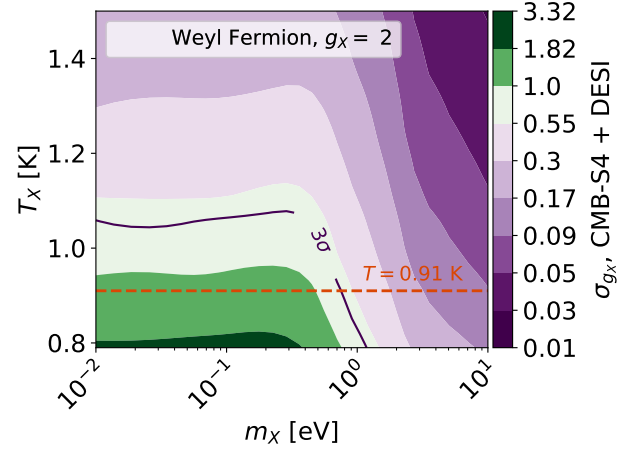


**FIG. 7:** Same as Fig. 5 for DESI + CMB-S4.

We also consider a Dirac fermion, with  $g_X = 4$  and mass  $m_X$ . In terms of the equivalent Weyl fermion, this corresponds to a temperature  $T_W^{\text{eq}} = 1.08$  K and mass  $m_W^{\text{eq}} = 1.19 m_X$ . In Fig. 8b, we show that the combined *Planck* and BOSS datasets are forecasted to observe or rule out such particles above 1.30 (1.12) eV at  $3\sigma$  significance. For *Planck* and DESI, the  $3\sigma$  constraint is lowered to 0.61 (0.52) eV. Interestingly, CMB-S4 data will enable the parameter space of Dirac fermions with any mass to be observed or ruled out at  $3\sigma$  significance when combined with LSS data from DESI.

### Bosonic Relics

We now move to bosonic degrees of freedom. First, we study a minimum-temperature real scalar, with  $s = 0$ ,  $g_X = 1$ , and mass  $m_X$ . This is equivalent to a Weyl relic with  $T_W^{\text{eq}} = 0.79$  K and  $m_W^{\text{eq}} = 1.01 m_X$ . We show in

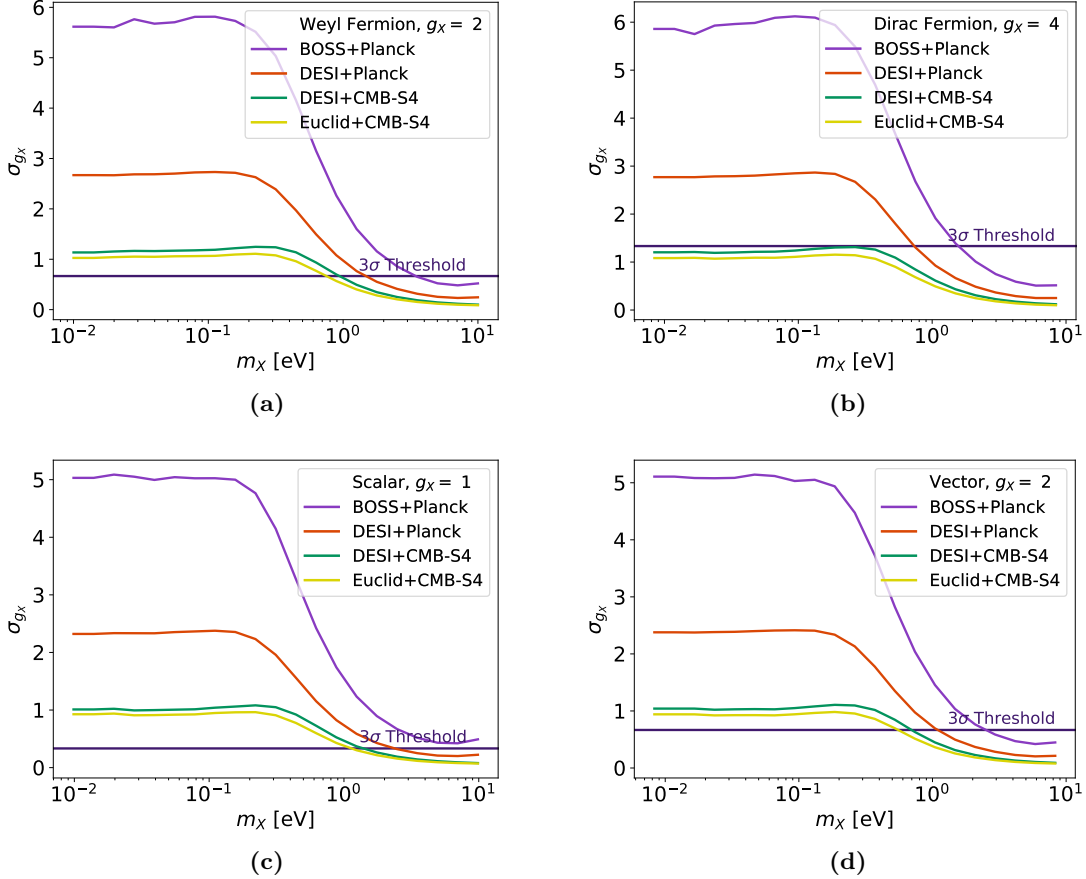


**FIG. 8:** Forecasted error on the relic degrees of freedom for a neutrino-like Weyl fermion (with fiducial  $g_X = 2$ , top left), a Dirac fermion ( $g_X = 4$ , top right), a real scalar ( $g_X = 1$ , bottom left), and a vector particle ( $g_X = 2$ , bottom right), all at their minimum temperature  $T_X = 0.91$  K, for various combinations of CMB + LSS experiments. The horizontal line denotes the uncertainty required to detect each relic at  $3\sigma$ .

Fig. 8c that, while the combination of presently available *Planck* and BOSS datasets cannot constrain scalar relics at the  $3\sigma$  significance, DESI and *Planck* can jointly rule out scalars with masses above 1.96 (1.61) eV. Further, the combination of CMB-S4 with either the DESI or *Euclid* datasets can observe or rule-out real scalar bosonic relics above 1.14 (1.06) and 0.93 (0.87) eV, respectively.

Second, we consider a massive vector, with  $s = 1$  and  $g_X = 2$ . This massive vector is equivalent to a Weyl relic with  $T_W^{\text{eq}} = 0.94$  K and  $m_W^{\text{eq}} = 1.21m_X$ . In Fig. 8d we show that the combination of *Planck* and BOSS datasets can observe or rule-out massive vector bosonic relics above 2.05 (1.79) eV, whereas substituting BOSS for DESI improves this number to 0.90 (0.75) eV. Combining the CMB-S4 and *Euclid* datasets further improves this to 0.47 (0.44) eV.

### C. Neutrino-mass forecasts

We have detailed in each previous subsection the constraints with and without marginalizing over neutrino masses to emphasize the importance of this step, as it is seen to affect results noticeably when LSS information is being considered. We note that DESI is particularly sensitive to the marginalization or fixing of  $\sum m_\nu$ . This is due to its chosen bias prescription, which does not include a parameter to marginalize over the redshift dependence of the bias, as opposed to BOSS and *Euclid*. This underscores the sensitivity of our results to the details of the bias prescription, which is further explored in our companion paper [47].

As a consequence of our analysis, we can also forecast how much neutrino-mass measurements would be affected by the presence of a LiMR, given the degeneracies between  $\sum m_\nu$  and  $g_X$  shown in Fig. 3. We show in Fig. 9 the relative increment in the error of the sum  $\sum m_\nu$  of neutrino masses when marginalizing over a relic

	CMB Only	BOSS	DESI	<i>Euclid</i>
Scalar $m_X$ [eV]				
LSS Only		- (-)	4.98 (4.54)	3.24 (3.22)
<i>Planck</i>	- (-)	- (-)	1.96 (1.61)	1.31 (1.16)
CMB-S4	1.48 (1.44)	1.41 (1.31)	1.14 (1.06)	0.93 (0.87)
Weyl Fermion $m_X$ [eV]				
LSS Only		- (-)	3.13 (2.78)	2.42 (2.41)
<i>Planck</i>	- (-)	2.85 (2.47)	1.20 (1.00)	0.87 (0.78)
CMB-S4	1.03 (1.02)	0.98 (0.91)	0.78 (0.71)	0.63 (0.59)
Vector $m_X$ [eV]				
LSS Only		- (-)	2.41 (2.08)	1.88 (1.88)
<i>Planck</i>	- (-)	2.05 (1.79)	0.90 (0.75)	0.65 (0.60)
CMB-S4	0.81 (0.78)	0.75 (0.70)	0.58 (0.54)	0.47 (0.44)
Dirac Fermion $m_X$ [eV]				
LSS Only		4.06 (3.72)	1.82 (1.36)	1.50 (1.50)
<i>Planck</i>	- (-)	1.30 (1.12)	0.61 (0.52)	0.45 (0.43)
CMB-S4	0.56 (0.55)	0.51 (0.48)	<b>All (All)</b>	<b>All (All)</b>

**TABLE III:** Minimum mass at which a LiMR (scalar boson, Weyl fermion, vector boson or Dirac fermion, from top to bottom) can be observed or ruled out at  $3\sigma$  significance. Also reported in parentheses is the result with fixed  $\sum m_\nu$  (to its fiducial value). A “-” sign corresponds to no masses within the  $3\sigma$  constraint. “**All**” corresponds to all LiMR masses analyzed being within the  $3\sigma$  constraint.

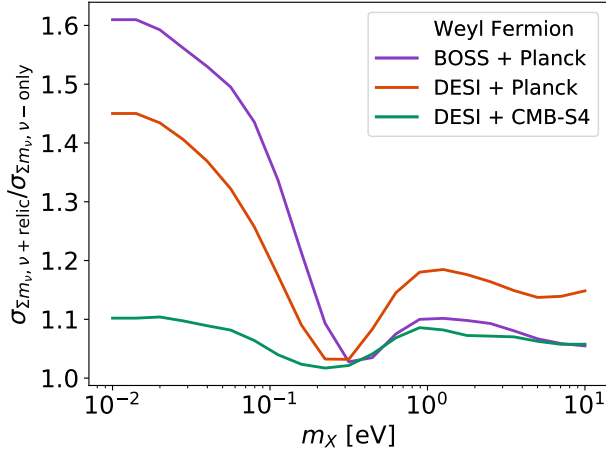


**FIG. 9:** Forecasted DESI + CMB-S4 uncertainty on the sum  $\sum m_\nu$  of neutrino masses, when it is jointly searched for with a relic of mass  $m_X$  and temperature  $T_X = 0.91$  K. The degeneracy is minimized at  $\sim \mathcal{O}(0.3\text{eV})$  for all particle types, although the constraints on neutrino masses using CMB data from *Planck* are always expected to weaken by  $\sim 10\%$ , if a new light relic is present.

of varying mass. For reference, we forecast  $\sigma(\sum m_\nu)$  to be 61.1 meV for BOSS and *Planck*, 28.2 meV for DESI and *Planck*, and 24.1 meV for DESI and CMB-S4, with a fiducial at the (normal-hierarchy) minimum  $\sum m_\nu = 60$  meV and no other relics. The degradation in the expected errors ranges from 10% for heavy relics and futuristic data (DESI+S4), to nearly 100% for lower masses

and current or upcoming data. (BOSS/DESI+*Planck*). We encourage the reader to see our companion paper [47] for in-depth neutrino forecasts without relics.

## V. CONCLUSIONS

In this work we have studied how well current and upcoming cosmological surveys can detect light (but massive) relics (LiMRs), focusing on the 10 meV to 10 eV mass range. These particles become non-relativistic before today, and thus affect the formation of structures in the universe. By combining information from the CMB and the LSS we have shown that a large swath of the 2D-parameter space (of relic mass and temperature) will be probed by upcoming surveys.

There is a minimum temperature that any relic that was in thermal equilibrium with the Standard Model should have,  $T_X^{(0)} = 0.91$  K. Interestingly, we find that Weyl, vectors, and Dirac relics with this temperature, and masses above  $\approx 1$  eV, can be observed or ruled out at the  $3\sigma$  significance using the presently available combination of *Planck* and BOSS datasets. Looking slightly to the future, the *Planck* and DESI datasets will improve these constraints, and reduce the minimum mass allowed for LiMRs by roughly 50%. The more futuristic *Euclid* and CMB-S4 datasets will present an 80% improvement and, in the case of Dirac fermions, fully cover the parameter space. If the sum of neutrino masses,  $\sum m_\nu$ , can be learned independently of CMB and LSS surveys, the effect of fixing the  $\sum m_\nu$  parameter manifests as an approximate 20% improvement on these constraints. We



emphasize that the effect of marginalizing  $\sum m_\nu$  significantly weakens the  $3\sigma$  constraints for some of the cases reported, suggesting that it is important to account for  $\sum m_\nu$  in any search for LiMRs. While the need to properly account for  $\sum m_\nu$  has been discussed in previous work [17, 26, 38, 87–89], our analysis, which does so for massive but light relics, is unprecedented.

This result is particularly interesting for the case of the gravitino. Since the gravitino would have a cosmological imprint identical to a Weyl fermion, we have shown that *Planck* and BOSS can observe or rule out gravitinos heavier than 2.85 eV. If a gravitino, or any other LiMR, were detected, then their parameters (i.e., mass and temperature) could also be measured, as suggested in Ref. [24].

In summary, while light relics are commonly assumed to be nearly massless — and constrained through  $N_{\text{eff}}$  —

here we have shown that relics with masses on the 10 meV to 10 eV scale can be constrained with cosmological data. These constraints are broadly expected to apply to the full range of allowed relic masses, from effectively massless to saturating the DM abundance. This complements current efforts in the search of relics, allowing many new routes for finding physics beyond the Standard Model.

## ACKNOWLEDGMENTS

We thank Sunny Vagnozzi for insightful comments on a previous version of this manuscript. We also thank Praatek Agrawal and David Pinner for discussions. ND was supported by a National Physical Science Consortium Graduate Fellowship for STEM Diversity. CD and JBM were partially supported by NSF grant AST-1813694.

- 
- [1] R. Peccei and H. R. Quinn, *Phys. Rev. Lett.* **38**, 1440 (1977).
  - [2] D. H. Weinberg, J. S. Bullock, F. Governato, R. Kuzio de Naray, and A. H. G. Peter, *Proc. Nat. Acad. Sci.* **112**, 12249 (2015), [arXiv:1306.0913 \[astro-ph.CO\]](#).
  - [3] P. Svrcek and E. Witten, *JHEP* **06**, 051 (2006), [arXiv:hep-th/0605206](#).
  - [4] A. Arvanitaki, S. Dimopoulos, S. Dubovsky, N. Kaloper, and J. March-Russell, *Phys. Rev. D* **81**, 123530 (2010), [arXiv:0905.4720 \[hep-th\]](#).
  - [5] S. Abel, M. Goodsell, J. Jaeckel, V. Khoze, and A. Ringwald, *JHEP* **07**, 124 (2008), [arXiv:0803.1449 \[hep-ph\]](#).
  - [6] T. Beranek, H. Merkel, and M. Vanderhaeghen, *Phys. Rev. D* **88**, 015032 (2013), [arXiv:1303.2540 \[hep-ph\]](#).
  - [7] N. Arkani-Hamed and N. Weiner, *JHEP* **12**, 104 (2008), [arXiv:0810.0714 \[hep-ph\]](#).
  - [8] R. Essig, P. Schuster, and N. Toro, *Phys. Rev. D* **80**, 015003 (2009), [arXiv:0903.3941 \[hep-ph\]](#).
  - [9] K. Cheung and T.-C. Yuan, *JHEP* **03**, 120 (2007), [arXiv:hep-ph/0701107 \[hep-ph\]](#).
  - [10] H. Goldberg and L. J. Hall, *Phys. Lett. B* **174**, 151 (1986).
  - [11] D. Feldman, Z. Liu, and P. Nath, *Phys. Rev. D* **75**, 115001 (2007), [arXiv:hep-ph/0702123 \[HEP-PH\]](#).
  - [12] S. Fukuda *et al.* (Super-Kamiokande), *Phys. Rev. Lett.* **85**, 3999 (2000), [arXiv:hep-ex/0009001 \[hep-ex\]](#).
  - [13] G. Mention, M. Fechner, T. Lasserre, T. A. Mueller, D. Lhuillier, M. Cribier, and A. Letourneau, *Phys. Rev. D* **83**, 073006 (2011), [arXiv:1101.2755 \[hep-ex\]](#).
  - [14] A. A. Aguilar-Arevalo *et al.* (MiniBooNE), *Phys. Rev. Lett.* **110**, 161801 (2013), [arXiv:1303.2588 \[hep-ex\]](#).
  - [15] M. Dentler, A. Hernández-Cabezudo, J. Kopp, P. A. N. Machado, M. Maltoni, I. Martinez-Soler, and T. Schwetz, *JHEP* **08**, 010 (2018), [arXiv:1803.10661 \[hep-ph\]](#).
  - [16] K. Benakli, Y. Chen, E. Dudas, and Y. Mambrini, *Phys. Rev. D* **95**, 095002 (2017), [arXiv:1701.06574 \[hep-ph\]](#).
  - [17] S. Bashinsky and U. Seljak, *Phys. Rev. D* **69**, 083002 (2004), [arXiv:astro-ph/0310198 \[astro-ph\]](#).
  - [18] Z. Hou, R. Keisler, L. Knox, M. Millea, and C. Reichardt, *Phys. Rev. D* **87**, 083008 (2013), [arXiv:1104.2333 \[astro-ph.CO\]](#).
  - [19] D. Baumann, D. Green, J. Meyers, and B. Walisch, *JCAP* **1601**, 007 (2016), [arXiv:1508.06342 \[astro-ph.CO\]](#).
  - [20] G. Mangano, G. Miele, S. Pastor, T. Pinto, O. Pisanti, and P. D. Serpico, *Nucl. Phys. B* **729**, 221 (2005), [arXiv:hep-ph/0506164 \[hep-ph\]](#).
  - [21] P. F. de Salas and S. Pastor, *JCAP* **07**, 051 (2016), [arXiv:1606.06986 \[hep-ph\]](#).
  - [22] N. Aghanim *et al.* (Planck), (2018), [arXiv:1807.06209 \[astro-ph.CO\]](#).
  - [23] A. Boyarsky, J. Lesgourgues, O. Ruchayskiy, and M. Viel, *JCAP* **0905**, 012 (2009), [arXiv:0812.0010 \[astro-ph\]](#).
  - [24] A. Banerjee, B. Jain, N. Dalal, and J. Shelton, *JCAP* **01**, 022 (2018), [arXiv:1612.07126 \[astro-ph.CO\]](#).
  - [25] J. Baur, N. Palanque-Delabrouille, C. Yèche, A. Boyarsky, O. Ruchayskiy, E. Armengaud, and J. Lesgourgues, *JCAP* **1712**, 013 (2017), [arXiv:1706.03118 \[astro-ph.CO\]](#).
  - [26] S. Dodelson, K. Heitmann, C. Hirata, K. Honscheid, A. Roodman, U. Seljak, A. Slosar, and M. Trodden, (2016), [arXiv:1604.07626 \[astro-ph.CO\]](#).
  - [27] D. Baumann, D. Green, and M. Zaldarriaga, *JCAP* **1711**, 007 (2017), [arXiv:1703.00894 \[astro-ph.CO\]](#).
  - [28] C. Brust, D. E. Kaplan, and M. T. Walters, *JHEP* **12**, 058 (2013), [arXiv:1303.5379 \[hep-ph\]](#).
  - [29] K. N. Abazajian *et al.* (CMB-S4), (2016), [arXiv:1610.02743 \[astro-ph.CO\]](#).
  - [30] R. H. Cyburt, B. D. Fields, K. A. Olive, and T.-H. Yeh, *Rev. Mod. Phys.* **88**, 015004 (2016), [arXiv:1505.01076 \[astro-ph.CO\]](#).
  - [31] C. Cheung, G. Elor, and L. Hall, *Phys. Rev. D* **84**, 115021 (2011), [arXiv:1103.4394 \[hep-ph\]](#).
  - [32] C. Dvorkin, T. Lin, and K. Schutz, *Phys. Rev. D* **99**, 115009 (2019), [arXiv:1902.08623 \[hep-ph\]](#).
  - [33] B. D. Fields, K. A. Olive, T.-H. Yeh, and C. Young, (2019), [arXiv:1912.01132 \[astro-ph.CO\]](#).
  - [34] G. Rossi, C. Yèche, N. Palanque-Delabrouille, and J. Lesgourgues, *Phys. Rev. D* **92**, 063505 (2015), [arXiv:1412.6763 \[astro-ph.CO\]](#).

- [35] N. Palanque-Delabrouille *et al.*, *JCAP* **11**, 011 (2015), [arXiv:1506.05976 \[astro-ph.CO\]](#).
- [36] S. Alam *et al.* (BOSS), *Mon. Not. Roy. Astron. Soc.* **470**, 2617 (2017), [arXiv:1607.03155 \[astro-ph.CO\]](#).
- [37] P. Zarrouk *et al.*, *Mon. Not. Roy. Astron. Soc.* **477**, 1639 (2018), [arXiv:1801.03062 \[astro-ph.CO\]](#).
- [38] D. Baumann, D. Green, and B. Wallisch, *JCAP* **1808**, 029 (2018), [arXiv:1712.08067 \[astro-ph.CO\]](#).
- [39] Y. Ali-Haïmoud and S. Bird, *Mon. Not. Roy. Astron. Soc.* **428**, 3375 (2012), [arXiv:1209.0461 \[astro-ph.CO\]](#).
- [40] S. Bird, Y. Ali-Haïmoud, Y. Feng, and J. Liu, *Mon. Not. Roy. Astron. Soc.* **481**, 1486 (2018), [arXiv:1803.09854 \[astro-ph.CO\]](#).
- [41] J. Lesgourgues and S. Pastor, *Phys. Rept.* **429**, 307 (2006), [arXiv:astro-ph/0603494 \[astro-ph\]](#).
- [42] D. Blas, J. Lesgourgues, and T. Tram, *JCAP* **1107**, 034 (2011), [arXiv:1104.2933 \[astro-ph.CO\]](#).
- [43] M. LoVerde and M. Zaldarriaga, *Phys. Rev. D* **89**, 063502 (2014), [arXiv:1310.6459 \[astro-ph.CO\]](#).
- [44] M. LoVerde, *Phys. Rev. D* **90**, 083530 (2014), [arXiv:1405.4855 \[astro-ph.CO\]](#).
- [45] J. B. Muoz and C. Dvorkin, *Phys. Rev. D* **98**, 043503 (2018), [arXiv:1805.11623 \[astro-ph.CO\]](#).
- [46] C.-T. Chiang, M. LoVerde, and F. Villaescusa-Navarro, *Phys. Rev. Lett.* **122**, 041302 (2019), [arXiv:1811.12412 \[astro-ph.CO\]](#).
- [47] W. L. Xu, N. DePorzio, J. B. Muoz, and C. Dvorkin, (2020).
- [48] P. J. E. Peebles, *Astrophys. J.* **146**, 542 (1966).
- [49] D. A. Dicus, E. W. Kolb, A. M. Gleeson, E. C. G. Sudarshan, V. L. Teplitz, and M. S. Turner, *Phys. Rev. D* **26**, 2694 (1982).
- [50] S. Bashinsky and U. c. v. Seljak, *Phys. Rev. D* **69**, 083002 (2004).
- [51] Z. Hou, R. Keisler, L. Knox, M. Millea, and C. Reichardt, *Phys. Rev. D* **87**, 083008 (2013), [arXiv:1104.2333 \[astro-ph.CO\]](#).
- [52] K. Osato, T. Sekiguchi, M. Shirasaki, A. Kamada, and N. Yoshida, *JCAP* **1606**, 004 (2016), [arXiv:1601.07386 \[astro-ph.CO\]](#).
- [53] S. P. Martin, “A Supersymmetry primer,” in *Perspectives on supersymmetry. Vol.2*, Vol. 21, edited by G. L. Kane (2010) pp. 1–153, [arXiv:hep-ph/9709356](#).
- [54] L. Covi, J. E. Kim, and L. Roszkowski, *Phys. Rev. Lett.* **82**, 4180 (1999), [arXiv:hep-ph/9905212](#).
- [55] M. Reece, *JHEP* **07**, 181 (2019), [arXiv:1808.09966 \[hep-th\]](#).
- [56] K. Abazajian *et al.*, *Bull. Am. Astron. Soc.* **51**, 209 (2019), [arXiv:1908.01062 \[astro-ph.IM\]](#).
- [57] K. S. Dawson, D. J. Schlegel, C. P. Ahn, S. F. Anderson, E. Aubourg, S. Bailey, R. H. Barkhouser, J. E. Bautista, A. Beifiori, A. A. Berlind, and et al., *The Astronomical Journal* **145**, 10 (2012).
- [58] A. Aghamousa *et al.* (DESI), (2016), [arXiv:1611.00036 \[astro-ph.IM\]](#).
- [59] L. Amendola *et al.*, *Living Rev. Rel.* **21**, 2 (2018), [arXiv:1606.00180 \[astro-ph.CO\]](#).
- [60] M. Archidiacono, S. Hannestad, and J. Lesgourgues, (2020), [arXiv:2003.03354 \[astro-ph.CO\]](#).
- [61] C. M. Hirata and U. Seljak, *Phys. Rev. D* **68**, 083002 (2003), [arXiv:astro-ph/0306354 \[astro-ph\]](#).
- [62] T. Okamoto and W. Hu, *Phys. Rev. D* **67**, 083002 (2003), [arXiv:astro-ph/0301031 \[astro-ph\]](#).
- [63] v. Ivezić *et al.* (LSST), *Astrophys. J.* **873**, 111 (2019), [arXiv:0805.2366 \[astro-ph\]](#).
- [64] T. Abbott *et al.* (DES), (2005), [arXiv:astro-ph/0510346 \[astro-ph\]](#).
- [65] A. Boyle and E. Komatsu, *JCAP* **1803**, 035 (2018), [arXiv:1712.01857 \[astro-ph.CO\]](#).
- [66] C. Modi, E. Castorina, and U. Seljak, *Mon. Not. Roy. Astron. Soc.* **472**, 3959 (2017), [arXiv:1612.01621 \[astro-ph.CO\]](#).
- [67] T. Sprenger, M. Archidiacono, T. Brinckmann, S. Clesse, and J. Lesgourgues, *JCAP* **1902**, 047 (2019), [arXiv:1801.08331 \[astro-ph.CO\]](#).
- [68] A. Font-Ribera, P. McDonald, N. Mostek, B. A. Reid, H.-J. Seo, and A. Slosar, (2013), [10.1088/1475-7516/2014/05/023](#), [arXiv:1308.4164](#).
- [69] M. Kamionkowski, A. Kosowsky, and A. Stebbins, *Phys. Rev. D* **55**, 7368 (1997), [arXiv:astro-ph/9611125](#).
- [70] M. Zaldarriaga and U. Seljak, *Phys. Rev. D* **55**, 1830 (1997), [arXiv:astro-ph/9609170](#).
- [71] M. Tegmark, *Phys. Rev. Lett.* **79**, 3806 (1997), [arXiv:astro-ph/9706198 \[astro-ph\]](#).
- [72] J. B. Muoz, E. D. Kovetz, A. Raccanelli, M. Kamionkowski, and J. Silk, *JCAP* **05**, 032 (2017), [arXiv:1611.05883 \[astro-ph.CO\]](#).
- [73] S. Galli, K. Benabed, F. Bouchet, J.-F. Cardoso, F. El-sner, E. Hivon, A. Mangilli, S. Prunet, and B. Wandelt, *Phys. Rev. D* **90**, 063504 (2014), [arXiv:1403.5271 \[astro-ph.CO\]](#).
- [74] N. Kaiser, *Mon. Not. Roy. Astron. Soc.* **227**, 1 (1987).
- [75] P. Bull, P. G. Ferreira, P. Patel, and M. G. Santos, *Astrophys. J.* **803**, 21 (2015), [arXiv:1405.1452 \[astro-ph.CO\]](#).
- [76] E. V. Linder, *Phys. Rev. D* **72**, 043529 (2005), [arXiv:astro-ph/0507263 \[astro-ph\]](#).
- [77] I. Zehavi *et al.* (SDSS), *Astrophys. J.* **571**, 172 (2002), [arXiv:astro-ph/0106476](#).
- [78] C. Alcock and B. Paczynski, *Nature* **281**, 358 (1979).
- [79] M. Asgari, A. Taylor, B. Joachimi, and T. D. Kitching, *Mon. Not. Roy. Astron. Soc.* **479**, 454 (2018), [arXiv:1612.04664 \[astro-ph.CO\]](#).
- [80] P. Lemos, A. Challinor, and G. Efstathiou, *JCAP* **1705**, 014 (2017), [arXiv:1704.01054 \[astro-ph.CO\]](#).
- [81] A. Moradinezhad Dizgah, H. Lee, J. B. Muoz, and C. Dvorkin, *JCAP* **05**, 013 (2018), [arXiv:1801.07265 \[astro-ph.CO\]](#).
- [82] T. Moroi, H. Murayama, and M. Yamaguchi, *Phys. Lett. B* **303**, 289 (1993).
- [83] A. Hook and H. Murayama, *Phys. Rev. D* **92**, 015004 (2015), [arXiv:1503.04880 \[hep-ph\]](#).
- [84] A. Hook, R. McGehee, and H. Murayama, *Phys. Rev. D* **98**, 115036 (2018), [arXiv:1801.10160 \[hep-ph\]](#).
- [85] M. Viel, J. Lesgourgues, M. G. Haehnelt, S. Matarrese, and A. Riotto, *Phys. Rev. D* **71**, 063534 (2005), [arXiv:astro-ph/0501562](#).
- [86] S. Deser and B. Zumino, *Phys. Rev. Lett.* **38**, 1433 (1977).
- [87] D. D. Baumann, F. Beutler, R. Flauger, D. R. Green, A. z. Slosar, M. Vargas-Magaa, B. Wallisch, and C. Yche, *Nature Phys.* **15**, 465 (2019), [arXiv:1803.10741 \[astro-ph.CO\]](#).
- [88] D. Green *et al.*, *Bull. Am. Astron. Soc.* **51**, 159 (2019), [arXiv:1903.04763 \[astro-ph.CO\]](#).
- [89] A. Font-Ribera, P. McDonald, N. Mostek, B. A. Reid, H.-J. Seo, and A. Slosar, *JCAP* **05**, 023 (2014), [arXiv:1308.4164 \[astro-ph.CO\]](#).

- [90] J. B. Muoz, D. Grin, L. Dai, M. Kamionkowski, and E. D. Kovetz, *Phys. Rev. D* **93**, 043008 (2016), [arXiv:1511.04441 \[astro-ph.CO\]](#).

## Appendix A: MCMC Validation of Fisher Forecasts

In this Appendix we show a comparison of our Fisher formalism and an MCMC analysis of the same mock data to confirm our Fisher analysis throughout the main text. In Fig. 10 we show the MCMC (solid) and Fisher forecasted (dotted) marginalized posteriors for cosmological parameters and nuisance parameters (including the neutrino mass  $\sum m_\nu$ ), assuming CMB-S4 + DESI data. This Figure shows that the predicted errors agree remarkably well between our Fisher-matrix approach and the full MCMC of mock data.

Moreover, we show posteriors for models with and without the growth induced scale-dependent modification to the bias (as described in our companion paper [47]), which we termed GISDB. The MCMC results are from Ref. [47], and the Fishers are calculated here. The non-GISDB Fisher ellipses are centered on the corresponding MCMC maximum likelihood point. The GISDB ones, however, are shifted by [90]

$$\delta\theta_i = (F^{-1})_{ij}D_j, \quad (\text{A1})$$

in each parameter  $\theta_i$ , where we have defined

$$D_j = \sum_z \int k^2 dk \int d\mu \frac{V(z)}{2(2\pi)^2} \left( \frac{\partial \log \tilde{P}_g(k, \mu)}{\partial \theta_j} \right) \left( \tilde{P}_{g, \text{GISDB}}(k, \mu) - \tilde{P}_{g, \text{no GISDB}}(k, \mu) \right) \left( \frac{\bar{n}\tilde{P}_g}{\bar{n}\tilde{P}_g + 1} \right)^2, \quad (\text{A2})$$

and the GISDB Fisher ellipses are computed centered on the shifted best-fit. As shown, the good cohesion between

the Fisher and MCMC analyses of the data, particularly in the inclusion of the GISDB effect, demonstrates that the considered effects are well-approximated by the linearity of the Fisher approach, and thus validates the constraints we present on additional light relics.

## Appendix B: Sampling of Full Model Posterior Forecasts

Datasets with different parameter degeneracies can powerfully constrain parameters when combined. To illustrate this complementary effect between CMB and LSS surveys, we present a sampling of fully marginalized posteriors in Fig. 11 for a Weyl (neutrino-like) relic with temperature 0.91 K and mass 0.01 eV. In each figure, we present constraints using only DESI (red), only *Planck* (violet), and the joint dataset (green).

As in the case of the LiMR parameter  $g_X$  (number of degrees of freedom) discussed in the main text, the addition of LSS information to CMB data will generally break degeneracies between parameters. As an interesting example, we observe that the LSS provides a measurement of  $\omega_{\text{cdm}}$  that is very close to orthogonal from the CMB one, breaking degeneracies with  $A_s$ ,  $n_s$  and  $g_X$  for very light relic masses. DESI information also serves to set the measurements on  $h$  and  $\sum m_\nu$ , which are poorly measured by *Planck* as their effects on the CMB are degenerate. In turn, the LSS by itself is generally ineffective at measuring the other cosmological parameters, and provides no information on  $\tau_{\text{reio}}$ . While, as illustrated in Fig. 3, the degeneracies between  $g_X$  and other parameters shift significantly between relics of different masses, those between the cosmological parameters themselves remain largely unchanged.

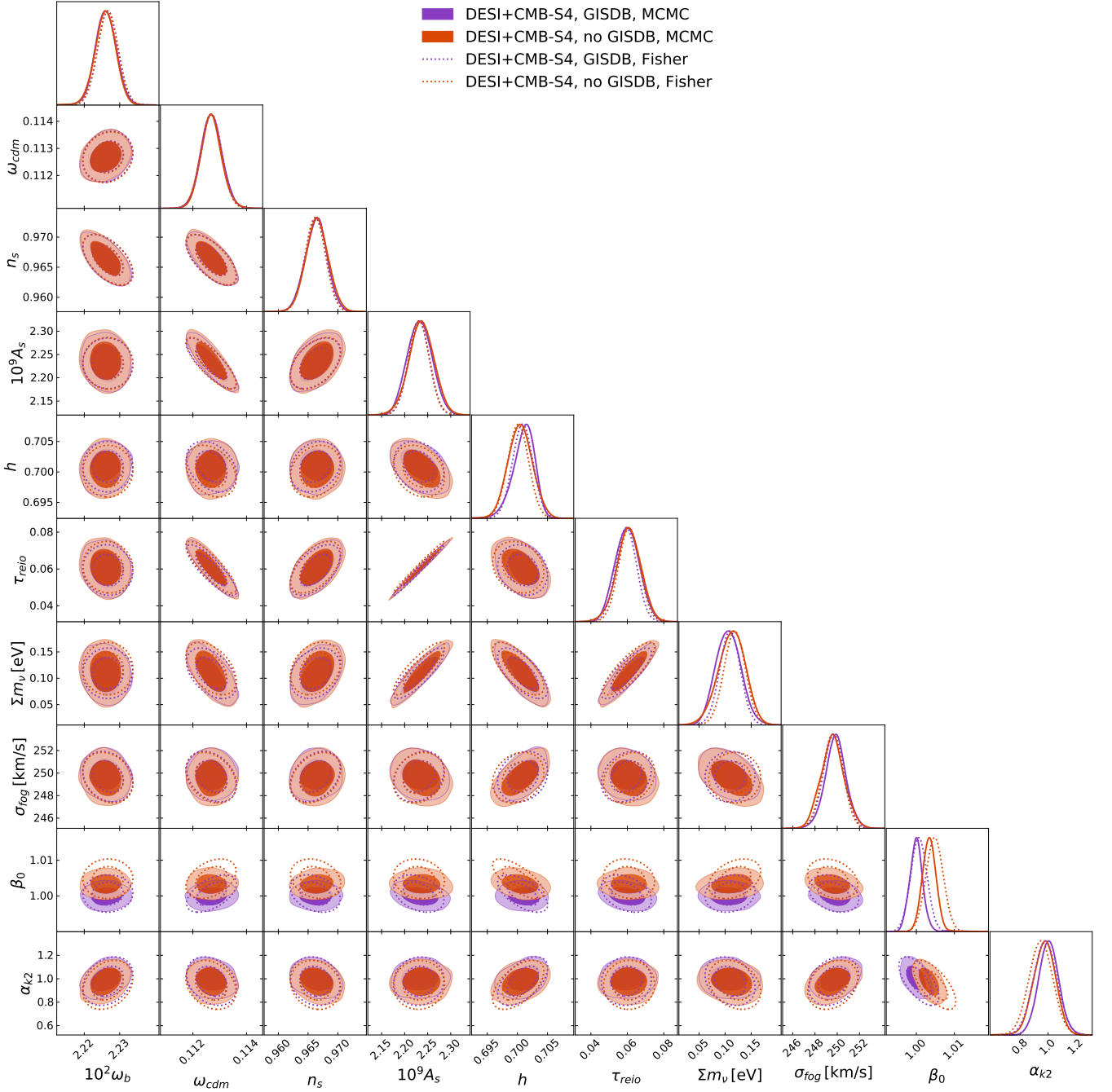


**FIG. 10:** MCMC and Fisher forecasted marginalized posteriors for cosmological parameters and nuisance parameters for a joint DESI + CMB-S4 analysis. The degenerate hierarchy is assumed with a total mass of  $\sum m_\nu = 100$  meV. Models with and without the bias step (GISDB) are considered. As shown, the good consistency between MCMC and Fisher results, particularly the reproduced shift in parameters upon turning off GISDB, demonstrates that the effects we consider are well-captured at linear order and validates our results regarding the detectability of LiMRs.



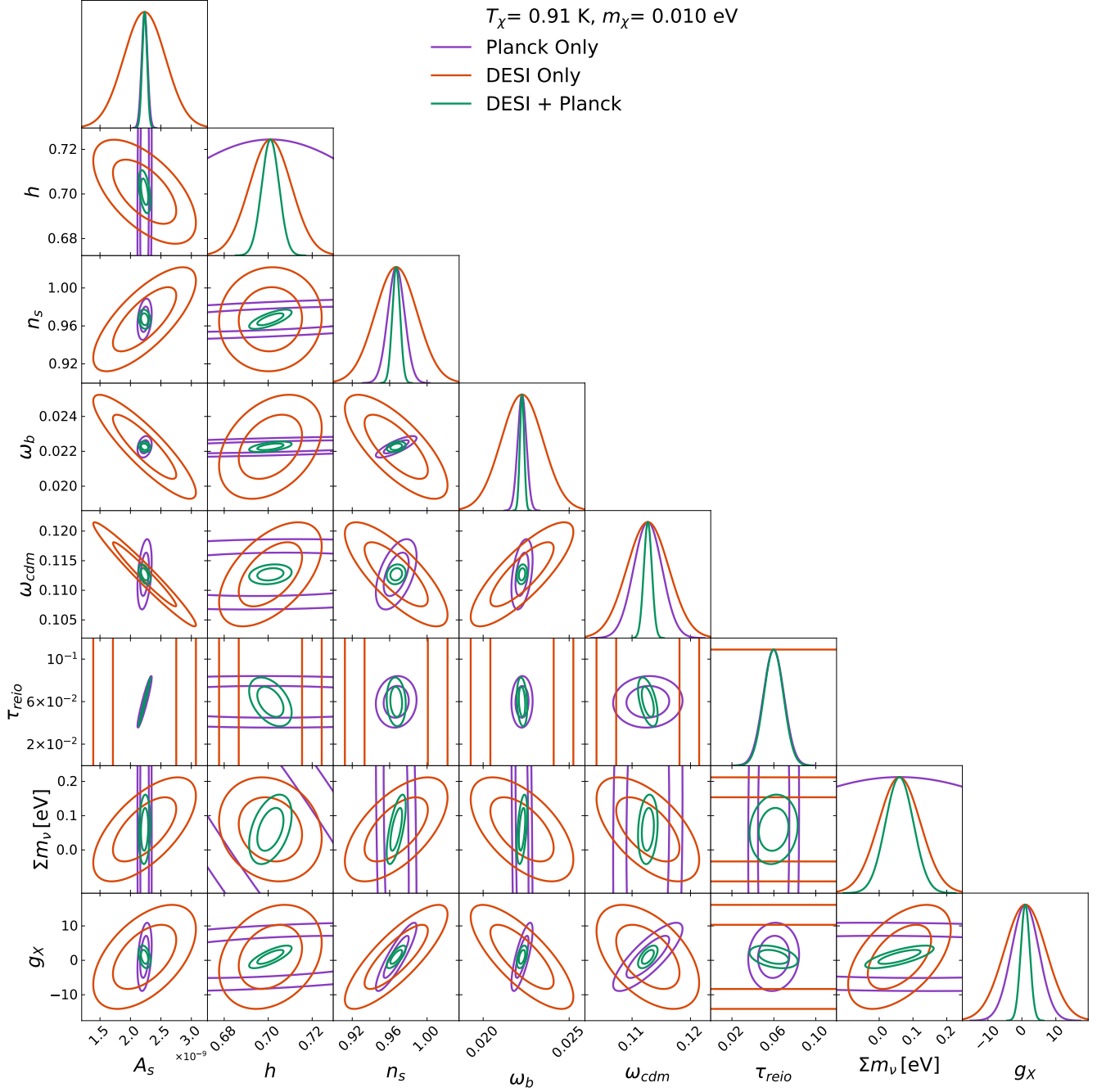


**FIG. 11:** 2-dimensional posterior distributions for parameter forecasts using DESI + *Planck*, and each experiment individually. We assume here the presence of a Weyl fermion LiMR ( $g_X = 2$ ) with  $T_X = 0.91 \text{ K}$  and  $m_X = 0.01 \text{ eV}$ . As shown, the complementarity between the two datasets results in marked improvement on the sensitivity to such a relic.